A Multi-Resolution Pyramid for Outdoor Robot Terrain Perception

Michael Montemerlo and **Sebastian Thrun**
AI Lab, Stanford University
353 Serra Mall
Stanford, CA 94305-9010
{mmde,thrun}@stanford.edu

Abstract

This paper addresses the problem of outdoor terrain modeling for the purposes of mobile robot navigation. We propose an approach in which a robot acquires a set of terrain models at differing resolutions. Our approach addresses one of the major shortcomings of Bayesian reasoning when applied to terrain modeling, namely artifacts that arise from the limited spatial resolution of robot perception. Limited spatial resolution causes small obstacles to be detectable only at close range. Hence, a Bayes filter estimating the state of terrain segments must consider the ranges at which that terrain is observed. We develop a multi-resolution approach that maintains multiple navigation maps, and derive rational arguments for the number of layers and their resolutions. We show that our approach yields significantly better results in a practical robot system, capable of acquiring detailed 3-D maps in large-scale outdoor environments.

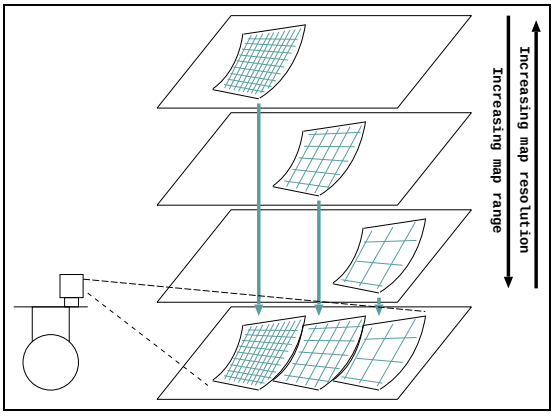

Figure 1: The terrain perception pyramid: terrain is modeled with multiple maps at differing resolutions, each sensitive to observations at different ranges.

Introduction

This paper addresses the problem of robots navigating through unknown terrain. This problem arises in great many robot applications, such as planetary exploration (Matthies *et al.* 1995) and the exploration of abandoned mines (Ferguson *et al.* 2003). In such cases, a robot must rely on its sensors to determine the location of obstacles, so as to safely navigate through free space. In indoor environments, this is commonly achieved by assuming the world is planar and estimating a 2-D cross-section of the environment (Borenstein & Koren. 1991; Burgard *et al.* 2000; Simmons *et al.* 2000; Yamauchi *et al.* 1998). Outdoor environments require a 3-D analysis of the ground and possible obstacles that might protrude into navigable space (Hashimoto & Yuta 2003; Matthies & Grandjean 1992). Of particular importance are *negative* obstacles, characterized by the absence of supporting ground (e.g., holes) (Matthies *et al.* 1998) as well as obstacles that might protrude into the robot's workspace from far above the ground (e.g., overhangs) (Ferguson *et al.* 2003).

When modeling the navigability of terrain, one common approach is to extract a navigability assessment from sensor measurements (e.g., range scans), and to integrate these assessment over time using Bayes filters. To perform this integration, existing techniques partition the workspace into a grid, similar to the well-known occupancy grid map algorithm (Moravec 1988). For each grid cell, sensor measurements are integrated using Bayes rule to diminish the effect of sensor noise.

Real-world terrain sensors have limited measurement resolution. For example, SICK laser range finders can only measure ranges with 0.5° accuracy; similar limitations exist for stereo camera systems and sonar sensors. Limited resolution can cause two problems with standard evidence grid algorithms:

1. First, the limited resolution may make it impossible to detect small obstacles at a distance. Obstacles like curbs or low-hanging wires can usually only be detected at close range. This is at odds with the ideal of Bayesian evidence integration in terrain grids: If evidence gathered at a distance *systematically* misses an obstacle, the grid may not change quickly enough when the robot is finally near the grid cell. As a result, the terrain model may miss obstacles, compromising the safety of the vehicle.
2. Second, limited sensor resolution makes it difficult to systematically find navigable terrain at a distance. As a result, a motion planner is either forced to make optimistic assumptions about the nature of terrain at a distance (with the obvious expense of having to replan when negative obstacles are encountered), or must remain confined to nearby regions that have been completely imaged.

The first limitation is the critical one that motivates our research, although our approach solves both of these problems.

The key insight in solving the first problem is to note that

the range at which terrain is analyzed plays a *systematic* role in the robot's ability to detect obstacles. To make this dependence explicit, we propose to maintain multiple terrain maps, each sensitive to different, possibly overlapping sensor ranges. This is illustrated in Figure 1: Terrain observations are incorporated into the maps sensitive to the range at which the observation was acquired. Each map, thus, models the probability of obstacles *detectable at a particular range*. When combining maps for assessing the navigability of terrain, preference is given to shorter range maps; however, all maps participate in motion planning.

The use of multiple maps raises the issue of their resolution. As we will show in this paper, a variable resolution approach yields superior coverage to a fixed resolution approach. To derive an appropriate resolution, we will analyze the effect of measurement noise and limited resolution on the density of measurements, so that the maximum resolution is chosen at each level that guarantees that all grid cells are covered with high likelihood. The result of this analysis is a pyramid of terrain maps: Near the robot we have a fine-grained map sufficient for maneuvering the robot in close proximity to obstacles, whereas the map far from the robot is coarse, facilitating the task of motion planning. In extensive experiments, we show that the resulting approach is superior to existing terrain modeling approaches, in that it enhances the robot's safety while facilitating motion planning.

Bayesian Techniques for Navigability

In this section we present our core Bayesian technique for constructing navigability maps of unknown terrain. The approach requires that the robot be equipped with a 3-D range finder. For a fixed resolution grid, this approach is identical to a previously published algorithm in (Ferguson *et al.* 2003). It forms the basis of the pyramid described in subsequent sections.

Suppose the robot acquires a 3-D range scan of its surrounding terrain. Each measurement is mapped into a $(x\ \ y\ \ z)$-coordinate using the obvious coordinate transformation. Whether or not a location $(x\ \ y)$ is navigable is determined by a simple geometric analysis; A location is navigable at height z if the z-values of all measurements in the vicinity of $(x\ \ y)$ are either near each other (e.g., less than 5cm deviation), or are above the ground plane at a distance that exceeds the height of the robot. Either criterion is easily verified by a simple geometric analysis, as shown in (Ferguson *et al.* 2003).

The analysis of navigability results in a probability distribution $p(x_i \mid z_t)$ for each nearby location x_i, conditioned on the range scan z_t (here t denotes the time). Multiple measurements covering the same grid cell are then integrated using Bayes rule:

$$p(x_i \mid z_1, z_2, \ldots, z_T) = \frac{p(z_T \mid x_i, z_1, \ldots, z_{T-1})\ p(x_i \mid z_1, \ldots, z_{T-1})}{p(z_T \mid z_1, \ldots, z_{T-1})} \quad (1)$$

The "standard" derivation of the algorithm assumes that x_i is a sufficient statistic of the past, hence we get

$$= \frac{p(z_T \mid x_i)\ p(x_i \mid z_1, \ldots, z_{T-1})}{p(z_T \mid z_1, \ldots, z_{T-1})} \quad (2)$$

and after another application of Bayes rule

$$= \frac{p(x_i \mid z_T)\ p(z_T)\ p(x_i \mid z_1, \ldots, z_{T-1})}{p(x_i)\ p(z_T \mid z_1, \ldots, z_{T-1})} \quad (3)$$

The navigability variable is binary—either a cell is navigable or not. Thus, we can invert the entire reasoning by substituting $\neg x_i$ for x_i:

$$p(\neg x_i \mid z_1, z_2, \ldots, z_T) = \frac{p(\neg x_i \mid z_T)\ p(z_T)\ p(\neg x_i \mid z_1, \ldots, z_{T-1})}{p(\neg x_i)\ p(z_T \mid z_1, \ldots, z_{T-1})} \quad (4)$$

If we now divide (3) by (4) and substitute $p(\neg x_i \mid \cdot) = 1 - p(x_i \mid \cdot)$ for arbitrary conditioning variables, we essentially obtain the standard grid mapping algorithm in (Moravec 1988), but here for navigability:

$$\frac{p(x_i \mid z_1, z_2, \ldots, z_T)}{1 - p(x_i \mid z_1, z_2, \ldots, z_T)} = \frac{p(x_i \mid z_T)}{1 - p(x_i \mid z_T)}\ \frac{1 - p(x_i)}{p(x_i)}\ \frac{p(\neg x_i \mid z_1, \ldots, z_{T-1})}{1 - p(\neg x_i \mid z_1, \ldots, z_{T-1})} \quad (5)$$

Or in log-form, with the recursion added out:

$$\log \frac{p(x_i \mid z_1, z_2, \ldots, z_T)}{1 - p(x_i \mid z_1, z_2, \ldots, z_T)} = \log \frac{p(x_i)}{1 - p(x_i)} + \sum_t \left[\log \frac{p(x_i \mid z_t)}{1 - p(x_i \mid z_t)} + \log \frac{1 - p(x_i)}{p(x_i)} \right] \quad (6)$$

This update equation—which simply adds or subtracts evidence for the navigability from each grid cell—is at the core of classical techniques with a single navigability grid (Ferguson *et al.* 2003; Hashimoto & Yuta 2003), as well as our new approach that maintains a pyramid of grids at different resolutions.

The key problem of this update lies in its implicit independence assumption. Consider a grid cell x_i that contains a non-navigable curb that can only be detected at close range. Measured from a distance, $p(x_i \mid z_t)$ will be smaller than the prior $p(x_i)$, hence

$$\frac{p(x_i \mid z_t)}{1 - p(x_i \mid z_t)} + \log \frac{1 - p(x_i)}{p(x_i)} \quad (7)$$

will be negative. Let this value be called α. At close range, the robot can detect the obstacles; hence this expression turns into a positive value. Let us call this positive value β. The posterior will only indicate occupancy if the number of close range readings is at least $n\frac{-\alpha}{\beta}$, where n is the number of long-range readings. Otherwise, the obstacle may be missed. Clearly, for any value of α and β, the approach can fail when the number of long-range readings is too large.

Multi-Resolution Approaches

The central idea of our paper is to develop a pyramid of terrain models, in which each terrain model captures the occupancy from measurement data acquired at different ranges. These maps are defined through a sequence of distances

$$0 = d_0 < d_1 < d_2 < \ldots < d_N = \max \text{dist} \quad (8)$$

that partition the space of all distances at which the robot can perceive, up to its maximum range. Each interval $[d_n; d_{n+1})$ defines a map, that is, at any point in time, our approach only updates a grid cell in the n-th map if the actual distance of this cell to the sensor (at the time of measurement) falls into

the interval $[d_n; d_{n+1})$. In this way, each range scan leads to updates at multiple maps.

The definition of the values $\{d_n\}$ requires some analysis, in that the issue of the grid resolution and the distance band to which each grid is tuned are closely intertwined. Our analysis will be carried out in two parts. First, we will derive a bound on the maximum resolution of each grid cell, which guarantees with high likelihood that all grid cells are covered. This bound sets the resolution levels at different ranges d_n; as to be expected, the resolution decreases with distance. The actual ranges $\{d_n\}$ that define the individual maps are then determined by an argument that ensures uniform spread of updates at all levels of the pyramid, which implies that all of the occupancy maps are similar in their resulting confidence.

Upper Bound for the Grid Resolution

In this section, we will derive an upper bound on the resolution of each grid cell as a function of the distance to the robot, d. This bound is derived as a lower bound on the grid resolution. The bound is driven by three considerations: the effects of measurement noise, the vertical resolution, and the horizontal resolution of the range scanning device. Its rationale is that for exploration, we would like to guarantee coverage of each grid cell with high likelihood. Part of our analysis requires a flat ground. This is because the curvature in front of the robot is generally unknown a priori.

The bound assumes a range sensor with vertical angular resolution of ϕ (e.g., 1 degree) and horizontal angular resolution ψ, which is mounted at a fixed height h on the robot. Let r_α be the correct measurement of a range finder pointed at the vertical angle α, where $\alpha = 0$ denotes the horizontal direction. On a flat surface, the exact range r_α is obtained by the following equation

$$r_\alpha \quad = \quad \frac{h}{\sin\alpha} \tag{9}$$

Sensor measurements are, of course, noisy. The actual sensor measurement is a probabilistic function of r_α. Let this distribution be denoted by $p(\hat{r}_\alpha \mid r_\alpha)$, where $\hat{r}_\alpha$ denotes the actual measurement. For our analysis, let us assume that the variance of this distribution is given by σ_r^2.

Let d be the horizontal distance of a grid cell to the robot. The measurement noise causes noise in the distance at which ground is detected. The variance of this distance d due to measurement noise is given by

$$\sigma_d^2 \quad = \quad \frac{\sigma^2}{1 + (\frac{h}{d})^2} \tag{10}$$

where σ^2 is the variance of $p(\hat{r}_\alpha \mid r_\alpha)$. To see this, we note that the measurement angle at distance d is

$$\alpha \quad = \quad \arctan\frac{h}{d} \tag{11}$$

Thus, range noise is projected onto surface noise in proportion to the cosine of this angle:

$$\begin{aligned} \cos\alpha \quad &= \quad \cos\left(\arctan\frac{h}{d}\right) \\ &= \quad \frac{1}{\sqrt{1 + (\frac{h}{d})^2}} \end{aligned} \tag{12}$$

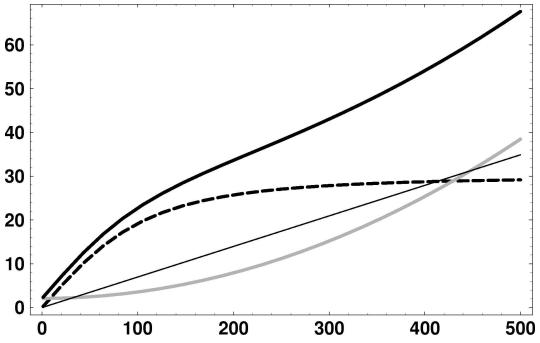

Figure 2: Lower bound on the grid cell size, for a range scanner with $\phi = 0.5^\circ$ vertical resolution, $\psi = 2^\circ$ horizontal resolution, and measurement noise $\sigma = 15$cm.

Since the variance is a quadratic function, the resulting variance on the ground is as stated in (10). For $d \gg h$, we have $\sigma^2 \approx \sigma_d^2$, suggesting a lower bound for the grid cell size that is asymptotically independent on the distance d.

This is quite different for the effect of limited angular resolution. Let ϕ be the vertical angular resolution of the sensor. Equation (11) specified the angle at which a point on the ground at distance d is detected. This angle is a function of d. Its dependence on d is characterized by the derivative

$$\left|\frac{\partial\alpha}{\partial d}\right| \quad = \quad \frac{h}{d^2 + h^2} \tag{13}$$

Thus, for any (small) angular resolution ϕ, we obtain

$$\Delta d \quad \approx \quad \phi\,\frac{(d^2 + h^2)}{h} \tag{14}$$

where Δd is the minimum vertical ground difference detectable by a sensor with resolution ϕ. This value is of course only an approximation, since the function α is approximated using a linear function (first order Taylor expansion). However, for small ϕ, this value gives us an accurate measure of the distance between ground detections due to sensor limitations. This value increases *quadratically* with the distance d.

The horizontal resolution of the scanner ψ gives us the relation

$$\frac{\Delta d}{2d} \quad = \quad \arctan\frac{\psi}{2} \tag{15}$$

and hence

$$\Delta d \quad = \quad 2d\arctan\frac{\psi}{2} \tag{16}$$

which grows linearly in d.

Since resolution and noise effects are all worst-case additive, an appropriate lower bound for the grid cell size is

$$\delta(d) \quad = \quad \frac{\sigma}{\sqrt{1 + (\frac{h}{d})^2}} + 2d\ \arctan\frac{\psi}{2} + \phi\,\frac{(d^2 + h^2)}{h} \tag{17}$$

which consists of a constant, a linear, and a quadratic term.

Figure 2 illustrates the lower bound on the grid cell size, for a vertical resolution $\phi = 0.5^\circ$, a horizontal resolution $\psi = 2^\circ$,

and a measurement noise variance $\sigma = 15$cm. The top curve is our additive lower bound, composed of the noise bound (dashed curve) that asymptotes into a constant, the linear horizontal resolution bound (thin line), and the resolution bound (gray curve) that grows quadratically. Within a range of up to five meters, the total bound is surprisingly close to a linear function. Beyond this range, it becomes quadratic.

As noted above, our analysis is based on the assumption of a flat ground. This assumption is adopted to reflect that the ground ahead of the robot is unknown. It is pessimistic in the face of an upward slope, in which case the density of measurements is larger than expected (hence the bound could be reduced). It is optimistic on downward-sloped ground, in which the resulting grid cells might not always be covered by at least one sensor measurement. In such situations, the robot will have to reduce its exploration speed so as to compensate the effects of reduced visibility in such terrain.

The Pyramid

We have just devised a lower bound on the grid cell size depending on the range d at which measurements are integrated. In this section, we will derive a rational argument for number and shape of the layers in our pyramid.

In determining the number of layers in the pyramid, we trade off the size of an obstacle that can be detected by the robot and the resolution and range at which it can be detected.

For a sensor with vertical resolution π, the ability to determine an obstacle of height Δz depends on the distance d. This height is easily determined using the obvious geometric equation:

$$\frac{\Delta z}{2d} \quad = \quad \arctan \frac{\phi}{2} \tag{18}$$

This implies that the height of detectable obstacles depends linearly on the distance d, for a sensor with fixed resolution:

$$\Delta z \quad = \quad 2d \, \arctan \frac{\phi}{2} \tag{19}$$

This linear dependence suggests a linear decrease of grid resolution in the pyramid—this is at stark contract of an exponential structure of most pyramids in the field of computer vision. In particular, we propose an obstacle grid pyramid of resolutions $\Delta d, \gamma \Delta d, 2\gamma \Delta d, 3\gamma \Delta d, \ldots$, for a linear scaling parameter γ. With such a linear increase in resolution, the corresponding range for each layer is determined by the bound in (20):

$$d_i \quad = \quad \min_{\Delta d} \delta(d) < i \, \gamma \, \Delta d \tag{20}$$

While this bound is generally quadratic, within a measurement range of 5 meters the function is approximately linear. Thus, with appropriate choice of the pyramid resolution γ, we obtain a pyramid that scales linearly in resolution, and where each layer focuses on an approximately linear distance of cells near the robot.

In our experiments, we found that a "soft" boundary works better than a hard boundary on the association of ranges d to a layer in the pyramid. In particular, when receiving range measurements that provide information on navigability at the distance d, the information integrated into the grid defined for the range d_i is gated by a factor of

$$\exp \left\{ -\tfrac{1}{2} \frac{(d - d_i)^2}{\sigma^2} \right\} \left[\log \frac{p(x_i \mid z_t)}{1 - p(x_i \mid z_t)} + \log \frac{1 - p(x_i)}{p(x_i)} \right]$$

Figure 3: The robotic vehicle is based on a Segway RMP, equipped with a vertically oriented SICK laser range finder mounted on an Amtec pan/tilt unit. The robot uses a highly tuned Inertial Measurement Unit and a GPS for localization.

This exponential decay leads to a smooth implementation of our distance-based multi-resolution grid approach.

Experimental Setup

We recently developed a mobile robot system for 3-D mapping and navigation of outdoor environments. Our navigation algorithm is described elsewhere (Likhachev, Gordon, & Thrun 2003): In essence, this approach finds a path through the map that maximizes the progress to a target location while minimizing the risks of encountering non-navigable space.

Our robot, shown in Figure 3, is based on the Segway RMP mobile platform. The RMP is a computer-controlled version of the commercial Segway HT scooter. The robot is equipped with a SICK laser range finder mounted on an Amtec pan-tilt unit. The laser is swept back and forth in order to acquire 3-D scans of the robot's environment. The robot also incorporates a sophisticated Inertial Measurement Unit (IMU) and GPS for localization. By projecting the endpoints of the laser scans into 3-D according to the estimated position of the robot and the angle of the pan-tilt, the robot can construct clouds of 3-D points describing the world around the robot.

By integrating constraints from the IMU, GPS, and matches between laser scans, we are able to construct large-scale, globally consistent, 3-D maps of urban environments. A map of the center of Stanford campus over 600 meters wide is shown in Figure 4. While such maps are necessary for planning global routes from one location to another, the robot must also monitor the immediate surroundings of the robot to ensure safe motion. The navigation pyramid algorithm described in this paper was implemented as the local navigation layer on the Segway. Experiments were performed to validate the two advantages of the pyramid algorithm: robustness to limited spatial resolution, and improved sensor coverage.

The first experiment is shown in Figures 5 to 7. Figure 5 shows the robot standing at a distance from a set of stairs. At this distance the robot is not able to detect the stairs as an obstacle. Both the standard evidence grid algorithm and the pyramid algorithm generate terrain maps like the one shown in Figure 5. (All levels of the pyramid were chosen to have a fixed resolution for the purposes of comparison with the stan-

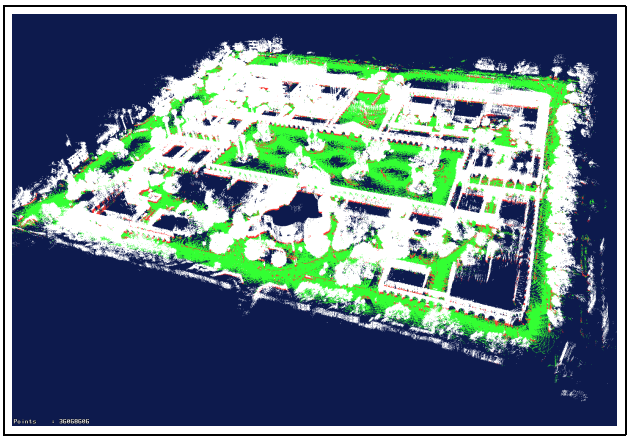

Figure 4: 3-D map of the center of the Stanford campus constructed by the Segway. The map is over 600 meters across, and was constructed from over 10 km of travel.

dard algorithm.) After standing still for several minutes, both algorithms describe the stairs area as being empty with high probability.

Subsequently, the robot was driven up to the stairs. At closer ranges, the stairs are detected as obstacles, but the standard evidence grid is unable to overcome the previous evidence describing the cells as free space. The resulting evidence grid, shown in Figure 6 does not contain the steps and would have resulted in a collision of the robot. The pyramid algorithm, on the other hand (Figure 7, was able to detect the stairs. As the robot moved closer to the stairs, the obstacles were incorporated into the shorter range layers of the terrain map.

The second experiment, pictured in Figures 8 and 9, shows an example of the effect of multi-resolution pyramids on mapping performance. Figure 8 shows a fixed resolution terrain map generated while the robot was approaching a gate. The localization of obstacles in the map is quite good, but the sweeping pattern of the laser leaves large holes in the terrain map. The abundance of holes makes it difficult to plan smooth local paths through this environment. Figure 9 shows the same scenario, except using a multi-resolution pyramid. Obstacles near the robot are precisely mapped, while obstacles in the distance are stored at low resolution. Furthermore, most of the holes in the terrain map have been filled.

Conclusion

This paper proposed a pyramid approach to acquiring terrain models with mobile robots. The model was motivated by a key flaw in flat grid approaches to modeling the navigability of terrain; namely, that the ability of a sensor to detect obstacles varies with range. By integrating information into a single flat map, failures to detect obstacles at a distance are treated as random noise, and not what they actually are: the systematic effect of limited sensor resolution.

Our approach alleviates this problem by devising a hierarchy of maps, each tuned to a different sensor range (and hence a different sensor resolution). We derive a mathematical bound that provides a rational argument for determining the region covered by each map, and the granularity of the grid cells in each map. As a result, the map resolution decreases with the measurement range, which has the nice side effect that the resulting maps tend to have much higher coverage than common single-map approaches.

We have demonstrated our approach using an actual outdoor mobile robot system. Our system is based on a robotic Segway scooter, and has successfully acquired large-scale models of areas $1km^2$ in size. Our experiments demonstrate that our approach successfully identifies obstacles in situations where the

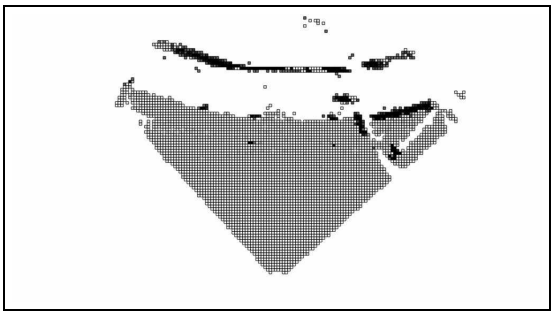

Figure 5: Watching the stairs from a distance, both algorithms create a similar terrain map with the stairs marked as free space.

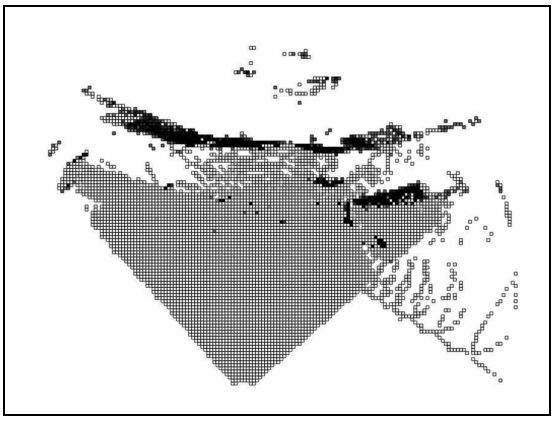

Figure 6: After the robot approaches the stairs, the standard occupancy grid algorithm is unable to overcome the previous negative evidence and the curb is not detected.

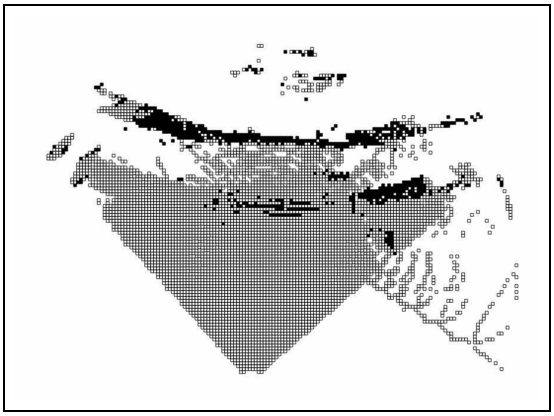

Figure 7: The pyramid approach is able to detect the stairs in time to safely avoid them.

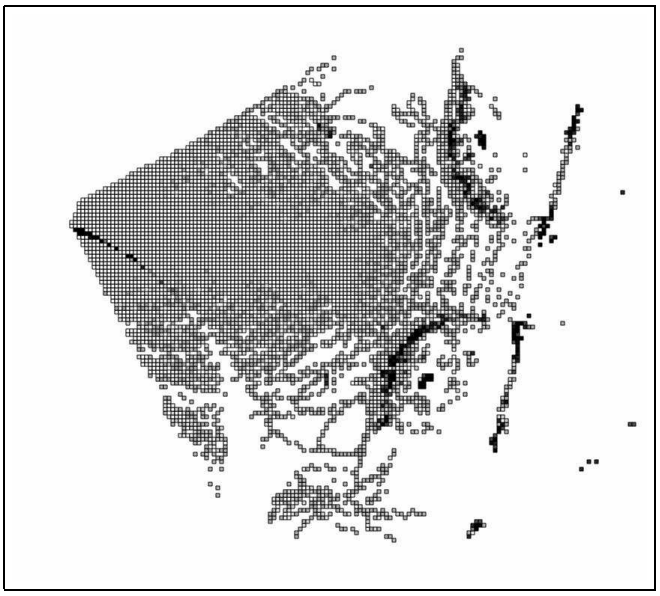

Figure 8: Model of the robot's surroundings using a fixed resolution grid. The large number of holes in the map makes motion planning difficult.

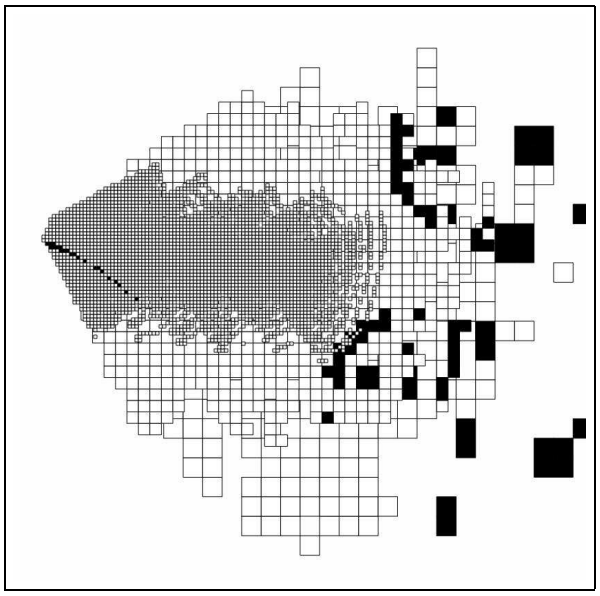

Figure 9: Multi-resolution pyramid model of the robot's surroundings. The majority of holes in the map are filled in. The terrain map close to the robot is very high resolution, while the area far from the robot is very coarse.

flat approach fails, and that it indeed leads to improved coverage in the resulting map. Computationally, our approach is only marginally more expensive than the single map approach, which should make our approach the method of choice for outdoor mobile robot navigation.

Acknowledgements

This research is sponsored by by DARPA's MARS Program (Contract number N66001-01-C-6018), which is gratefully acknowledged.

References

Borenstein, J., and Koren., Y. 1991. The vector fi eld histogram – fast obstacle avoidance for mobile robots. *IEEE Journal of Robotics and Automation* 7(3):278–288.

Burgard, W.; Fox, D.; Moors, M.; Simmons, R.; and Thrun, S. 2000. Collaborative multi-robot exploration. In *ICRA*. San Francisco, CA: IEEE.

Ferguson, D.; Morris, A.; Hähnel, D.; Baker, C.; Omohundro, Z.; Reverte, C.; Thayer, S.; Whittaker, W.; Whittaker, W.; Burgard, W.; and Thrun, S. 2003. An autonomous robotic system for mapping abandoned mines. In Thrun, S.; Saul, L.; and Schölkopf, B., eds., *NIPS*. MIT Press.

Hashimoto, K., and Yuta, S. 2003. Autonomous detection of untraversability of the path on rough terrain for the remote controlled mobile robots. In *Proceedings of the International Conference on Field and Service Robotics*.

Likhachev, M.; Gordon, G.; and Thrun, S. 2003. ARA*: Anytime A* search with provable bounds on sub-optimality. In Thrun, S.; Saul, L.; and Schölkopf, B., eds., *NIPS*. MIT Press.

Matthies, L., and Grandjean, P. 1992. Stereo vision for planetary rovers: Stochastic modeling to near real-time implementation. *International Journal of Computer Vision* 8(1):71–91.

Matthies, L.; Gat, E.; Harrison, R.; Wilcox, B.; Volpe, R.; and Litwin, T. 1995. Mars microrover navigation: Performance evaluation and enhancement. *Autonomous Robots* 2(4):291–311.

Matthies, L.; Litwin, T.; Owens, K.; Rankin, A.; Murphy, K.; Coorobs, D.; Gilsinn, J.; Hong, T.; Legowik, S.; Nashman, M.; and Yoshimi, B. 1998. Performance evaluation of ugv obstacle detection with ccd/flir stereo vision and ladar. In *Proceedings of the Joint Conference on the Science and Technology of Intelligent Systems*.

Moravec, H. P. 1988. Sensor fusion in certainty grids for mobile robots. *AI Magazine* 9(2):61–74.

Simmons, R.; Apfelbaum, D.; Burgard, W.; Fox, D. an Moors, M.; Thrun, S.; and Younes, H. 2000. Coordination for multi-robot exploration and mapping. In *Proceedings of the AAAI National Conference on Artificial Intelligence*. Austin, TX: AAAI.

Yamauchi, B.; Langley, P.; Schultz, A.; Grefenstette, J.; and Adams, W. 1998. Magellan: An integrated adaptive architecture for mobile robots. Technical Report 98-2, Institute for the Study of Learning and Expertise (ISLE), Palo Alto, CA.